# Preparation and thermal properties analysis of fatty acids/1-hexadecanol binary eutectic phase change materials reinforced with $TiO_2$ particles

Ruiqi Zhang[a], Dongming Chen[a], Lei Chen[b,*], Xing Cao[a,*], Xuebing Li[b], Yongtao Qu[c]

[a]*College of Electromechanical Engineering, Qingdao University of Science and Technology, Qingdao 266061, China*

[b]*Key Laboratory of Biofuels, Qingdao Institute of Bioenergy and Bioprocess Technology, Chinese Academy of Sciences, Qingdao 266101, China*

[c]*Department of Mathematics, Physics and Electrical Engineering, Northumbria University, Newcastle upon Tyne, NE1 8ST, United Kingdom*

**ABSTRACT**

Thermal energy storage with phase change materials (PCMs) is of great concern for energy conservation due to its characteristics of high latent heat and constant temperature during phase transition process. In this paper, binary eutectic mixtures (EMs) using fatty acids including lauric acid (LA), myristic acid (MA), palmitic acid (PA) and stearic acid (SA) with 1-hexadecanol (HD) are produced, and then titanium dioxide ($TiO_2$) is employed to form composite phase change materials (CPCMs) for purpose of promoting the thermal conductivity. The chemical structure, microscopic morphology, thermal property, thermal reliability and thermal stability of these CPCMs are inspected carefully. The results illustrate that $TiO_2$ particles have no obvious aggregation in EMs, and there is no chemical reaction between the components of CPCMs. High latent heats above 200 J/g are achieved with phase transition temperatures at 45.4 ℃, 51.2 ℃, 55.1 ℃ and 58.3 ℃ for individual system of LA-HD/$TiO_2$, MA-HD/$TiO_2$, PA-HD/$TiO_2$ and SA-HD/$TiO_2$ respectively. The prepared CPCMs maintain good performance after 100 thermal cycles. The decomposition of CPCMs is retarded and the thermal stability is enhanced. $TiO_2$ improves the thermal conductivities of EMs, which reach a maximum value of 0.358 W/(m·K). In brief, the CPCMs proposed in this paper possess high latent heat and high thermal conductivity as well as excellent thermal stability and thermal reliability, implying that it has a significant potential for thermal regulation and energy conservation.

**Keywords:**

Composite phase change materials

Fatty acid

1-Hexadecanol

Eutectic mixture

Thermal conductivity enhancement

*Corresponding authors.

*E-mail addresses:* chenlei@qibebt.ac.cn (L. Chen), caoxing@qust.edu.cn (X. Cao).

## 1. Introduction

Over the past few decades, environmental protection and energy utilization have been the most concerned issues around the world with the increasing economy development and population growth [1-3]. Especially for energy utilization, the potent utilization of abundant energy sources

including solar energy depends on an efficient and economical thermal storage technology called thermal energy storage (TES), which uses the storage media for storing surplus thermal energy during the heat absorption period and releasing when needed [4]. Of the feasible TES technology, the latent heat thermal energy storage (LHTES) has been demonstrated to be one of the powerful approaches for efficient energy storage and conversion. The storage medium of LHTES technology is the phase change material (PCM). PCM utilizes its properties of high latent heat and stable phase transition temperature during the thermal energy storage/release process to achieve high density energy storage and reduce temperature fluctuation [5-7]. Therefore, the PCM is widely used in various applications such as building energy conservation [8, 9], waste heat recovery [10], solar energy utilization [11], energy storage system [12, 13] and fabrics [14-16].

The PCMs include organic and inorganic types. Among organic PCMs, there are non-paraffin and paraffin materials. Compared with paraffin which comes from petroleum, the non-paraffin including fatty acids and fatty alcohols can be extracted from living resources without the consumption of fossil fuels. They exhibit abounding advantageous properties, typically good thermal and chemical stability, high latent heat storage capacity, suitable phase transition temperature, no super-cooling and phase separation, low price, non-toxicity and non-corrosiveness [17-19].

However, the phase transition temperatures of fatty acids and fatty alcohols are generally higher than what would be anticipated, which restrains their utilization in some specific situations, especially the residence and building heating. In order to deal with this dilemma, two or more types of fatty acids and their derivatives can be mixed as the eutectic mixture (EM) with stable feature via melting blending. The EM has a single melting/freezing point, which is lower than that of individual component. The phase transition temperature of PCM can be regulated to the suitable value of application by preparing EM [18, 20]. In recent years, numerous researches have been conducted concerning the fatty acids or fatty alcohols based EMs. Rezaie et al. [21] focused on myristic-lauric acid and myristic-stearic acid eutectic phase change materials. According to the experimental results, the composites have an appropriate and wider range of phase transition temperatures from 29.4 ℃-34.2 ℃ to 35.7 ℃-52.7 ℃. The corresponding enthalpies are 40.3 J/g-53.9 J/g and 41.9 J/g-55.0 J/g, respectively. The prepared composites can be utilized for low temperature energy storage/release systems. Hekimoğlu et al. [22] designed the lauric-myristic acid eutectic PCM and added it to the fly ash to make novel composite. The composite containing 27 wt.% lauric-myristic acid has a melting temperature of 31.1 ℃ and latent heat capacity of 45.3 J/g. The experimental results showed that this material has suitable phase transition temperature, good thermal and mechanical properties, which can be used for thermal regulation and energy saving in building. Jin et al. [8] prepared a novel composite of capric-stearic acid/montmorillonite. The DSC results manifested that the composite has a suitable phase transition temperature and high latent heat. The prepared composite retains the satisfactory phase change properties after 300 thermal cycles. Jebasingh et al. [20] focused on the development of capric-myristic acid EM. The prepared material maintains a high latent heat of 156.99 J/g and its phase transition temperature which is 20.86 ℃ decreases significantly relative to that of that of individual fatty acids. Cai et al. [23] fabricated a novel composite through combining the EM of capric-lauric-palmitic acid and $SiO_2$ nanofibers. The phase transition temperature of prepared EM is lower than that of individual fatty acids. After 50 thermal cycles, there are no obvious variations on the phase transition temperature and latent heat. Wei et al. [24] developed a form-stable PCM through employing the

capric-myristic-stearic acid EM and acid treated expanded vermiculite/carbon, which has good thermal and chemical stabilities. The melting temperature and latent heat of identified PCM is 22.92 ℃ and 86.4 J/g. Philip et al. [25] employed the dodecanol and hexadecanol to generate a EM, their results proved that this material with high thermal conductivity is suitable for low temperature energy storage. Philip et al. [26] prepared binary EM with lauryl alcohol and stearyl alcohol, which can be use in indoor thermal comfort in buildings. The experimental results demonstrated that the melting point of EM is 22.93 ℃, and the latent heat is 205.79 J/g. Liu et al. [27] prepared the myristic acid-tetradecanol EM, which has good thermal stability and is suitable for the building. DSC test indicated that the melting temperature and melting enthalpy of the PCM are 33.9 ℃ and 227.08 J/g respectively. Nevertheless, fewer researches have been focused on the preparation of fatty acids-fatty alcohols based EMs. The study of this type of EMs can help develop novel organic phase change materials and further enrich the phase transition temperature range of fatty acids and fatty alcohols.

Although fatty acids, fatty alcohols and their EMs display good properties, they still suffer from the similar demerit of low thermal conductivity like other organic PCMs. The usual solution is to incorporate the high-conductivity additives including particles of metals and metal oxides into PCMs. Rezaie et al. [19] prepared the shape-stable nano $Fe_3O_4$/fatty acids/PET composite. The addition of $Fe_3O_4$ nanoparticles increased thermal conductivity by approximately 44.5-85.8%. This composite can be utilized more efficiently for saving applications and thermal energy management. Teng et al. [28] prepared the composite PCMs (CPCMs) by adding $Al_2O_3$, $TiO_2$, $SiO_2$ and ZnO to the paraffin at 1.0 wt.%, 2.0 wt.% and 3.0 wt.%, respectively. The experimental results illustrated that $TiO_2$ is more effective than other particles in improving the thermal conductivity of paraffin. Harikrishnan et al. [29] selected lauric acid-stearic acid EM as base material, then added 1.0 wt.% $TiO_2$, 1.0 wt.% ZnO and 1.0 wt.% CuO in it respectively. Through comparing the results of the test, CuO is selected as the additive, which has the most significant enhancement of the base material's thermal conductivity. The obtained CPCM is suitable for the building heating applications. Kalaiselvam et al. [30] considered the n-tetradecane-n-hexadecane as a control material, then dispersed 0.07 wt.% $Al_2O_3$ and the same mass fraction of Al nanoparticles in it formed two types of CPCMs to enhance the thermal conductivity. The experimental results have proved that the solidification processes of CPCMs are more efficient comparing to the control material. The solidification time is reduced by 12.97% and 4.97% compared to the n-tetradecane-n-hexadecane, respectively. Sharma et al. [31] made CPCMs by adding different mass fractions of $TiO_2$ nanoparticles to palmitic acid. The experimental results showed that the CPCM with 0.5 wt.%, 1 wt.%, 3 wt.% and 5 wt.% $TiO_2$ intensify the thermal conductivity by 12.7%, 20.6%, 46.6% and 80% respectively compared to the palmitic acid base material. In addition, there are many other effective solutions, typically adding expanded graphite [32, 33], carbon nanotubes [34-36] and expanded perlite [24, 37, 38] to the organic PCM, which have positive effects on improving the thermal properties of organic PCMs. $TiO_2$ has received a lot of attention due to its high thermal conductivity, good thermal stability and other excellent properties [19, 39]. However, most of the available literature on it has investigated the effect of different $TiO_2$ additions on PCMs, while there is little literature on the experimental determination of $TiO_2$ additions and little literature on the performance-enhancing effects of $TiO_2$ on EMs (a series of fatty acids/1-hexadecanol binary eutectic mixtures) from the performance and cost perspective. Therefore, the paper is dedicated to the study of this issue.

Nevertheless, the thermally conductive particles tend to aggregate and settle in PCMs, which will deteriorate the stability of CPCMs. The electrostatic repulsion and spatial potential resistance possessed of dispersants make them be powerful adjuvants that can improve the dispersion of particles in solid or liquid, thus avoiding the particles aggregating and settling. The dispersants used so far are commonly polyvinylpyrrolidone [40], carboxymethylcellulose [41], sodium dodecylbenzene sulfonate [42] and cetyltrimethylammonium bromide [43].

Therefore, this study is devoted to the preparation of the novel CPCMs of fatty acids/1-hexadecanol (i.e., LA-HD/$TiO_2$, MA-HD/$TiO_2$, PA-HD/$TiO_2$ and SA-HD/$TiO_2$). Adding $TiO_2$ to enhance the EMs' thermal conductivity while using carboxymethylcellulose (CMC) to improve the dispersion of $TiO_2$. The chemical structure and microscopic morphology of the materials are observed through FTIR and SEM, the thermal properties and thermal stability of the materials are investigated by DSC and TGA. In order to test the thermal reliability of materials, 100 thermal cycles are implemented by the thermal cycling test. The thermal conductivities of the materials are measured with a thermal conductivity tester.

## 2. Experimental

### 2.1. Materials

Lauric acid (LA, $C_{12}H_{24}O_2$, AR), myristic acid (MA, $C_{14}H_{28}O_2$, AR), palmitic acid (PA, $C_{16}H_{32}O_2$, AR), stearic acid (SA, $C_{18}H_{36}O_2$, AR), 1-hexadecanol (HD, $C_{16}H_{34}O$, AR) and carboxymethylcellulose sodium (CMC-Na, $[C_6H_7O_2(OH)_2OCH_2COONa]_n$, AR) are obtained from Macklin. Titanium oxide ($TiO_2$, AR) is purchased from Tianjin Bodi Chemical Co., Ltd. $TiO_2$ has a bulk density of 4.26 g/$cm^3$ and an average particle size of 1~2 μm. It has a superhydrophilic surface with surface acidity and surface electrical property. It is used as a thermal conductive because of its high thermal conductivity (6.5 W/(m·K)). The materials utilized in this paper are used directly without any treatment.

### 2.2. Preparation of the composite phase change materials

In the present work, a series of fatty acids/1-hexadecanol CPCMs modified by fixed content of $TiO_2$ are experimentally synthesized. Eutectic composition and the content of additive added of the mixture are to be determined experimentally. A certain amount of fatty acid (i.e., LA, MA, PA or SA) and 1-hexadecanol are evenly mixed in a beaker at 70 ℃. The binary EMs as the base materials are stirred with 2 wt.% $TiO_2$ and 4 wt.% CMC at 70 ℃ using a glass rod and ultrasonically shaken for 10 min. The developed CPCMs are slowly cooled and dried in thermostatic chamber at room temperature. The preparation process is diagrammed in Fig. 1.

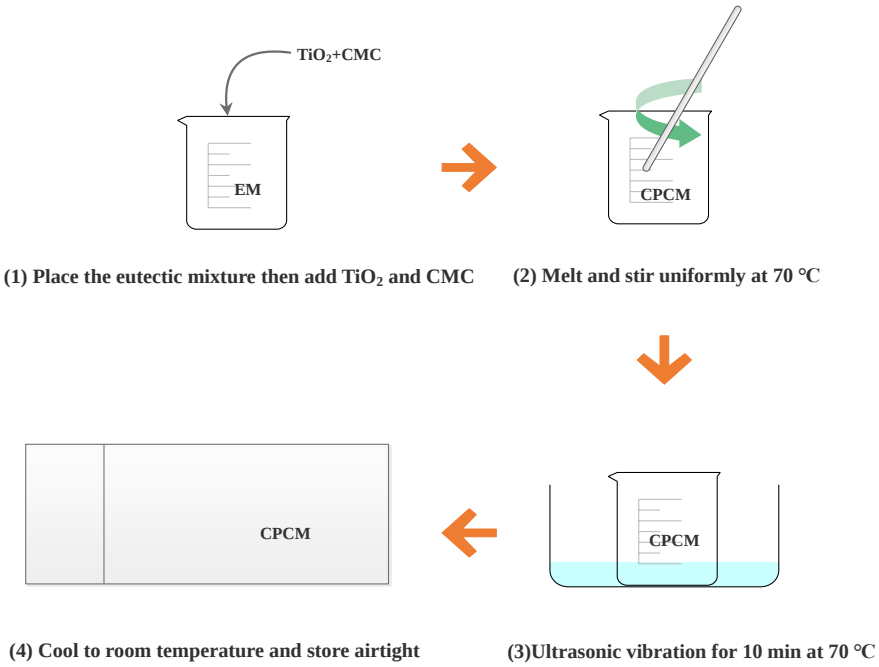


**Fig. 1.** The preparation process of composite phase change materials.

2.3. Characterization

Fourier transform infrared spectroscopy (FTIR, Nicolet 6700 spectrometer, United States) is used to test the absorption spectra of MA-HD, $TiO_2$, CMC and MA-HD/$TiO_2$ at 4000-500 $cm^{-1}$ with 2 $cm^{-1}$ resolution using KBr disk. The scanning electron microscopy (SEM, S4800, Japan) is used to analyze the microscopic morphology of $TiO_2$, CMC, LA-HD/$TiO_2$, MA-HD/$TiO_2$ PA-HD/$TiO_2$ and MA-HD/$TiO_2$. The working voltage is 5 kV. To avoid unclear pictures due to low electronic conductivity, all samples are treated with gold spray. The EDS-mapping (EDS, EX-37001, Japan) is used to observe the distribution of Ti in the sample MA-HD/$TiO_2$ under an accelerating voltage of 10 kV. In order to verify the feasibility of the Schrader equation calculation method for determining the parameters of fatty acids/1-hexadecanol, the step-cooling curve test is performed. The entire system consists of an Agilent data acquisition module (Agilent 34970A, United States), a computer terminal and a thermostatic water bath (DF-101S, China). The samples (i.e., MA, MA-HD with different mass ratios) are weighed 20 g each in six 50 mL beakers with an electronic balance. Put them into a constant temperature water bath to melt completely to reach thermal equilibrium then insert a K-type thermocouple into the middle of the sample. Finally, the samples are removed and cooled to room temperature. The temperature curves of the whole cooling process are recorded. The different mass ratios of $TiO_2$ and CMC are used in settling test to explore the stabilities of CPCMs. The samples of each group are stirred well and ultrasonically shaken in a water bath with a constant temperature at 70 ℃. Then, the samples are set in thermostatic chamber at 70 ℃ for 5 h. The settling phenomenon of the different samples is then compared. The simultaneous thermal analyzer (STA, HCT-1, China) is used for DSC analysis of thermal properties of PCMs, including extrapolated peak onset temperature, melting peak temperature and latent heat capacity. The phase change temperature mentioned in the text is melting peak temperature. The test is measured at a heating rate of 10 ℃/min from 30 ℃ to 100 ℃ in nitrogen atmosphere at 100 mL/min flow speed. After the set value has been reached, the temperature remains constant for 3 min. Each sample ranging from 3 mg to 8 mg is precisely

weighed through the electronic balance and sealed in the centre of a crucible made of aluminum oxide. The experiments are repeated for five times on each sample. The thermal cycling test is as follows: the CPCMs in the beakers are placed into a thermostatic chamber. The CPCMs are heated above the melting temperature. After reaching the set value, the temperature is kept constant for 10 min. Then cooled to room temperature and held for 30 min. Treating this process as one thermal cycle and repeating 100 times. The thermo gravimetry analysis (TGA) is performed by a simultaneous thermal analyzer (STA, HCT-1, China). The test is conducted at a heating rate of 10 ℃/min (nitrogen as the cooling medium) in the temperature range of 50-400 ℃ for studying the thermal stability of the base materials and composites. Samples are weighed and sealed in the same way as DSC measurements. Thermal conductivities of the EMs and CPCMs are determined by using TC3000D (XIATECH, China) thermal properties analyzer based on transient hot-wire method at room temperature. The accuracy of the test is ±3% and the measurements are repeated five times for ensuring the accuracy. The instrument is preheated for 30 min before measurement. The experimental voltage is 1 V during measurement and data acquisition of 2 s duration is performed every 3 min and repeated 5 times. The CPCMs are made into two cakes of the same size with a diameter of 50 mm and a thickness of 10 mm. Polishing them lightly with sandpaper. Then, the test sensor is clamped between the samples to ensure that the hot wire is completely covered by the samples, and thus measurements are performed.

## 3. Results and discussion

### 3.1. The composition of fatty acids/1-hexadecanol composite phase change materials

#### 3.1.1. Determination of eutectic composition

Depended on the lowest eutectic point theory, the eutectic mass ratio of mixture could be obtained through the Schrader equation as following [44].

$$T_{ab} = [\frac{1}{T_i} - \frac{R \ln X_i}{\Delta H_i}]^{-1} (i = a, b) \quad (1)$$

where $a$ or $b$ is one of the component in the binary EM, $T_{ab}$ is the phase transition temperature of the binary EM, $T_i$ and $\Delta H_i$ are the phase transition temperature and latent heat of $i$ respectively, $X_i$ is the mole fraction of $i$ and $R$ is the gas constant. The data used for the calculation are shown in Table 1.

**Table 1**

Phase transition temperature and enthalpy of the fatty acids and 1-hexadecanol.

| Sample | Melting temperature (℃) | Enthalpy (J/g) | Molecular weight |
|---|---|---|---|
| LA | 51.3 | 194.0 | 200.32 |
| MA | 63.3 | 197.3 | 228.37 |
| PA | 69.4 | 240.0 | 256.42 |
| SA | 77.6 | 244.0 | 284.48 |
| HD | 58.7 | 219.7 | 242.50 |

The results of the equation are fitted to two curves as shown in Fig. 2. The vertical coordinate of the intersection of two lines represents the eutectic temperature, and the horizontal coordinate shows the molar ratio of fatty acids. It can be seen from Fig. 2 that the theoretically eutectic temperatures of LA-HD, MA-HD, PA-HD and SA-HD are 41.85 ℃, 48.35 ℃, 52.35 ℃ and 55.15 ℃ respectively. The molar ratios of two components are 64.65:35.35, 47.47:52.53,

32.32:67.68 and 20.20:79.80, which indicates that the mass ratios are 60.17:39.83, 45.98:54.02, 36.64:63.36 and 22.90:77.10 respectively.

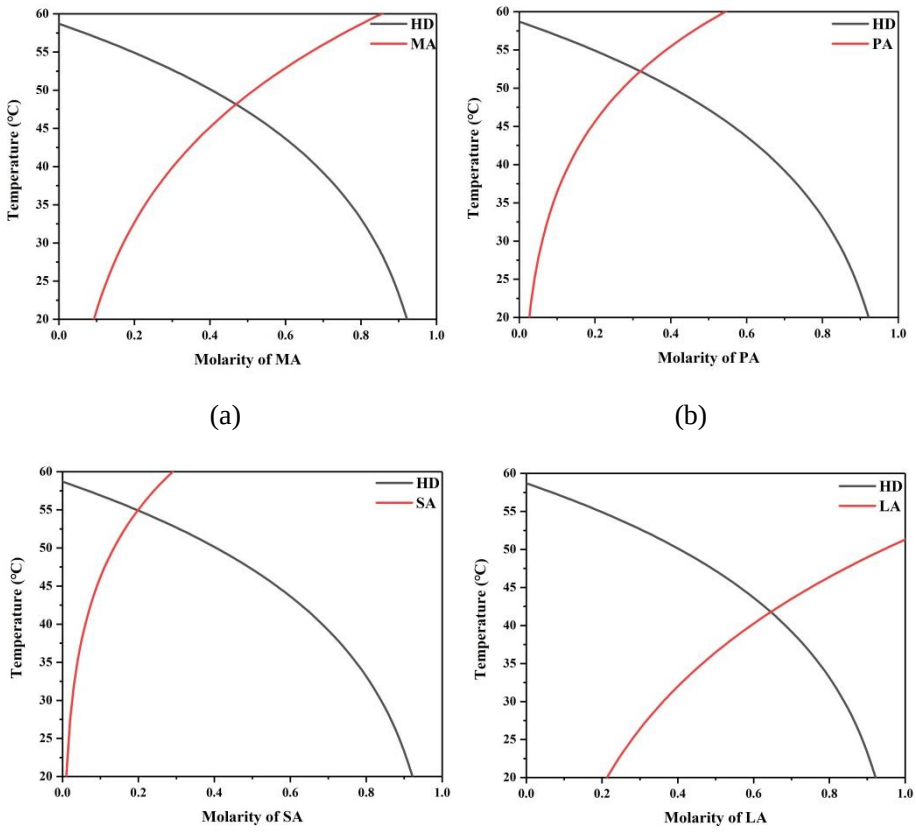


(a) (b)

(c) (d)

**Fig. 2.** The calculated results of eutectic temperatures and component molar ratios by Schrader equation. (a) MA-HD. (b) PA-HD. (c) SA-HD. (d) LA-HD.

In order to verify whether this calculation method is feasible for determining the parameters of fatty acids/1-hexadecanol, five samples with different mass ratios are prepared as shown in Table 2. All samples are tested for step cooling curves. The test results are illustrated in Fig. 3. The results showed that the MA-HD has a lower phase transition temperature than MA. The temperature changing gradually slows down and an obvious temperature plateau (as marked in Fig. 3) appears during the phase transition process, which lasts for about 2500 s. It demonstrates that the binary EM can effectively prolong the phase change process of MA, thus maintaining a constant temperature environment more efficiently.

**Table 2**

The MA-HD samples with different proportions.

| Sample | Mass ratio |
|---|---|
| 1 | 35.98：64.02 |
| 2 | 40.98：59.02 |
| 3 | 45.98：54.02 |
| 4 | 50.98：49.02 |
| 5 | 55.98：44.02 |

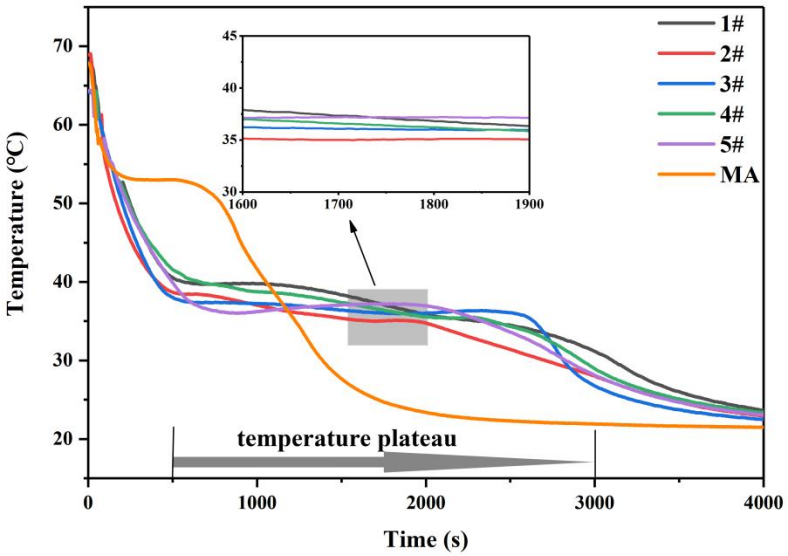


**Fig. 3.** The step cooling curves of samples.

To further determine the sample with the most stable feature, DSC test is performed on three samples (i.e., Sample 2, Sample 3 and Sample 4) with the relative lowest phase transition temperatures. This test is conducted in a pure nitrogen environment by maintaining a nitrogen flux of 100 mL/min and performed a heating process from 10 ℃ to 70 ℃ at a heating rate of 2 ℃/min. The test results are depicted in Fig. 4. Sample 3 has a single heat absorption peak with a sharp and smooth shape, which signifies that the sample 3 is completely eutectic and stable. MA and HD are fused into a whole material at this ratio. The component mass ratio of sample 3 is 45.98:54.02. It is consistent with the component mass ratio calculated theoretically, indicating that the Schrader equation is applicable. It is proved that the Schrader equation can be used for determining the eutectic compositions of fatty acids/1-hexadecanol. The properties of the fatty acids/1-hexadecanol EMs obtained from the calculations are listed in Table 3.

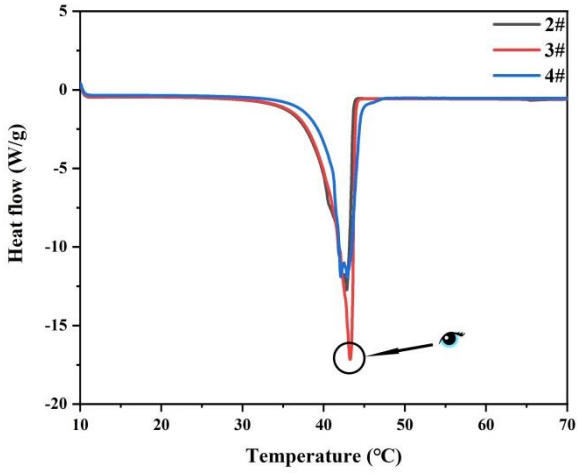


**Fig. 4.** The DSC curves of samples.

**Table 3**

The calculation results for eutectic mixtures.

| Eutectic mixture | Mass ratio | Eutectic temperature ( ℃) | Latent heat of phase change (J/g) |
|---|---|---|---|
| LA-HD | 60.17:39.83 | 41.85 | 196.98 |
| MA-HD | 45.98:54.02 | 48.35 | 201.67 |

| | | | |
|---|---|---|---|
| PA-HD | 36.64:63.36 | 52.35 | 219.71 |
| SA-HD | 22.90:77.10 | 55.15 | 222.54 |

3.1.2. Determination of the content of additive added

In order to improve the thermal conductivity of EMs, $TiO_2$ is added for improvement while CMC is selected to improve the dispersion of $TiO_2$. The effects of different mass ratios of $TiO_2$ and CMC on the stability of CPCMs are investigated. The mass ratios of $TiO_2$ and CMC in each sample are 1:1, 1:2, 1:3, 1:4 and 1:5 respectively. Due to EMs' analogous physical properties, MA-HD is selected as the representative matrix in this paper. The content of $TiO_2$ and CMC at different mass ratios is tabulated in Table 4. The samples of each group are stirred well and ultrasonically shaken in a water bath with a constant temperature at 70 ℃. Then, the samples are set in thermostatic chamber at 70 ℃ for 5 h. The phenomenon of settling test is shown in Fig. 5. Sample (a) has precipitation at the bottom of the test tube. The amount of CMC addition in this sample is the least, indicating that the content of CMC added in this ratio is not enough to disperse $TiO_2$ completely. Sample (c) displays a slight stratification. However, the stratification is more obvious in sample (d) and sample (e). When the content of CMC is too high, CMC in the lower part of the test tube due to its high density, which could form a layer of shadow area. The higher content of CMC is, the more obvious this phenomenon is. Therefore, too low/high content of CMC will cause a negative effect on CPCMs. The overall dispersion of sample (b) is homogeneous. The CPCM in this mass ratio is neither precipitated nor stratified. Therefore, the mass ratio of $TiO_2$ to CMC of 1:2 is decided.

**Table 4**

The content of $TiO_2$ and CMC with different mass ratios.

| Sample | $TiO_2$ content | CMC content |
|---|---|---|
| a | 2 wt.% | 2 wt.% |
| b | 2 wt.% | 4 wt.% |
| c | 2 wt.% | 6 wt.% |
| d | 2 wt.% | 8 wt.% |
| e | 2 wt.% | 10 wt.% |

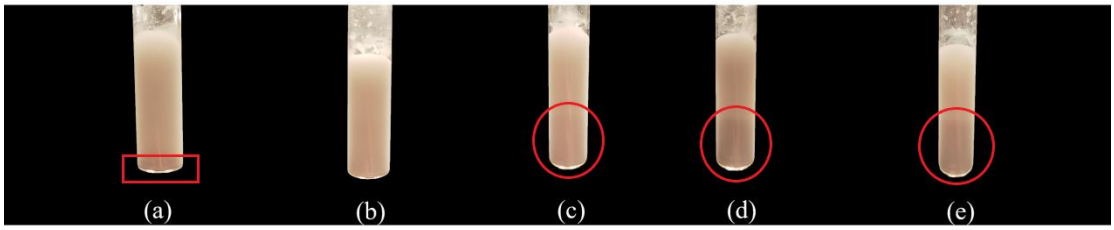


**Fig. 5.** The phenomenon of settling test.

Then the effect of $TiO_2$ content on the thermal conductivity needs to be determined. According to the above analysis, it is necessary to control the mass ratio of $TiO_2$ to CMC of 1:2 to make $TiO_2$ disperse completely and prevent the stratification phenomenon. Four groups of samples are set up accordingly. The thermal conductivities of four samples are tested by a thermal conductivity meter (TC3000D, China). The content of additive and the results of the test are seen in Table 5. When 2 wt.% $TiO_2$ is added, the thermal conductivity of MA-HD/$TiO_2$ reaches 0.320 W/(m·K), which is 8.47% higher than that of MA-HD. Moreover, with the increase of $TiO_2$ content, the improvement of thermal conductivity slows down clearly according to Fig. 6(b). Dramatic increase in thermal

conductivity is thus not expected even continue to increase the content of $TiO_2$. Therefore, 2 wt.% $TiO_2$ and 4 wt.% CMC are determined as additive for the fatty acids/1-hexadecanol EMs considering the balance between performance and cost.

**Table 5**

The content of additive and the results of test.

| Sample | $TiO_2$ content | CMC content | Thermal conductivity (W/(m·K)) | Degree of improvement |
|---|---|---|---|---|
| I | 0 | 0 | 0.295 | 0 |
| II | 0.5 wt.% | 1 wt.% | 0.313 | 6.10% |
| III | 1 wt.% | 2 wt.% | 0.317 | 7.46% |
| IV | 2 wt.% | 4 wt.% | 0.320 | 8.47% |

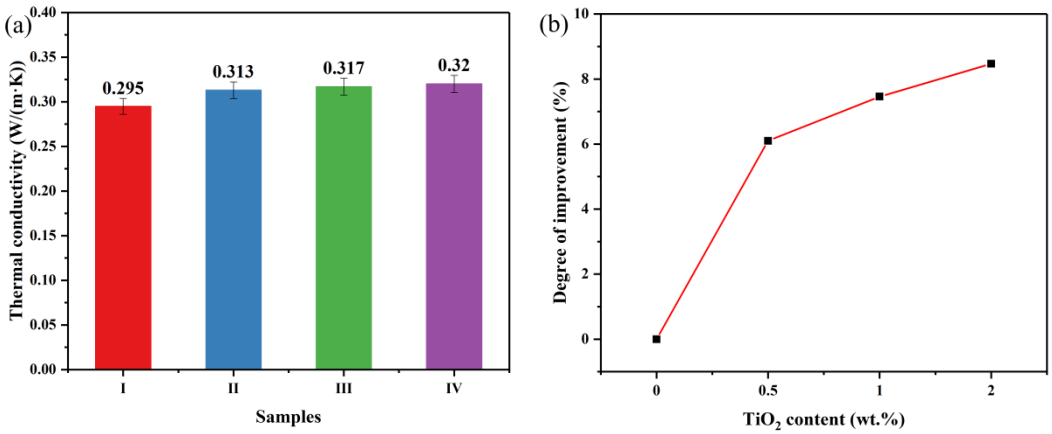


**Fig. 6.** (a) The thermal conductivity of four groups of samples and (b) the degree of improvement with different $TiO_2$ contents.

3.2. FTIR analysis

Previous report [32] has shown that the binary EM formed by fatty acids and fatty alcohols is simply physical blended without chemical reaction. Fig. 7 exhibits the FTIR spectra of MA-HD, $TiO_2$, CMC and MA-HD/$TiO_2$. In the spectrum of MA-HD, the peak at 2955.29 $cm^{-1}$ is assigned to the asymmetrical stretching vibration of $–CH_3$. The peaks at 2917.77 $cm^{-1}$ and 2849.75 $cm^{-1}$ are the asymmetrical stretching vibration and symmetrical stretching vibration of $–CH_2$, respectively. The peak which is the typical peak of MA at 1702.12 $cm^{-1}$ is attributed to the stretching vibration of –C=O. The peak at 1471.09 $cm^{-1}$ is corresponded to variable angle vibration of $–CH_2$ and asymmetric variable angle vibration of $–CH_3$. The peak which is the typical peak of HD at 1091 $cm^{-1}$ is stretching vibration of C–O. The peak at 720.33 $cm^{-1}$ is the in-plane swing vibration of $–(CH_2)_n–$. In the spectrum of the $TiO_2$, 1428.69 $cm^{-1}$ and 712.36 $cm^{-1}$ are corresponded to the asymmetric stretching and symmetric stretching vibration of Ti–O–Ti, respectively. In the spectrum of the CMC, the peak at 3472.62 $cm^{-1}$ indicates that there is stretching vibration bond of –OH. The peak at 1630.15 $cm^{-1}$ indicates that there is stretching vibration of –C=O. The peak at 1420.38 $cm^{-1}$ is corresponded to variable angle vibration of $–CH_2$. The peak at 1058.86$cm^{-1}$ is attributed to the stretching vibration of C–O.

The spectrum of MA-HD/$TiO_2$ has the similar characteristic peaks of MA-HD, $TiO_2$ and CMC. It's also found that there is no other obvious characteristic peak appeared or disappeared, which implies that no chemical interaction occurs in the mixing process of MA-HD, $TiO_2$ and CMC. Because of the similar properties, this conclusion is also applicable to CPCMs based on LA-HD, PA-HD and SA-HD.

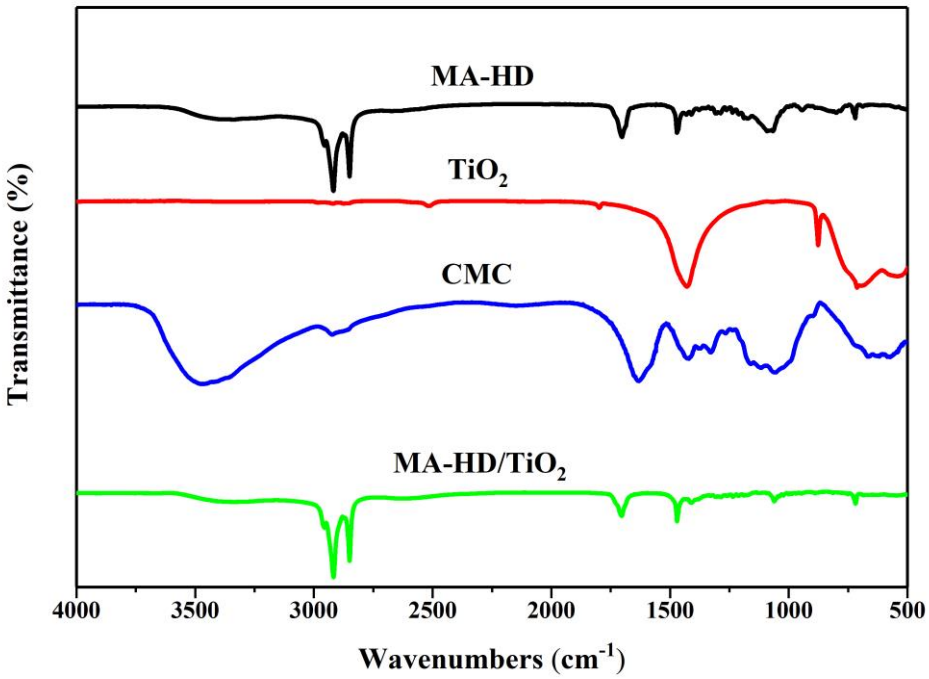


**Fig. 7.** The FTIR results of MA-HD, $TiO_2$, CMC and MA-HD/$TiO_2$.

3.3. SEM analysis and EDS-mapping

The SEM images of $TiO_2$, CMC, LA-HD/$TiO_2$, MA-HD/$TiO_2$, PA-HD/$TiO_2$, SA-HD/$TiO_2$ and the EDS-mapping results are depicted in Fig. 8. Fig. 8(a) shows that $TiO_2$ is the tiny particle with 2 μm. Fig. 8(b) shows that the CMC has the loose rod structure. In Fig. 8(c-f), the microstructures of four CPCMs with layered structure are revealed. A part of $TiO_2$ has been marked by white circles. The CMC allows the $TiO_2$ particles to be dispersed without obvious aggregation in the CPCMs. This is the result of the repulsive bond of surfactant [31]. MA-HD/$TiO_2$ is used as an example to illustrate this effect. As shown in Fig. 8(g-h), a good distribution state of Ti is observed from the EDS-mapping results, thus demonstrating a good distribution state of $TiO_2$. The tiny particle size of $TiO_2$ and the layered structure of CPCMs are effective in increasing the specific surface area, which have a positive effect on enhancing the thermal conductivity.

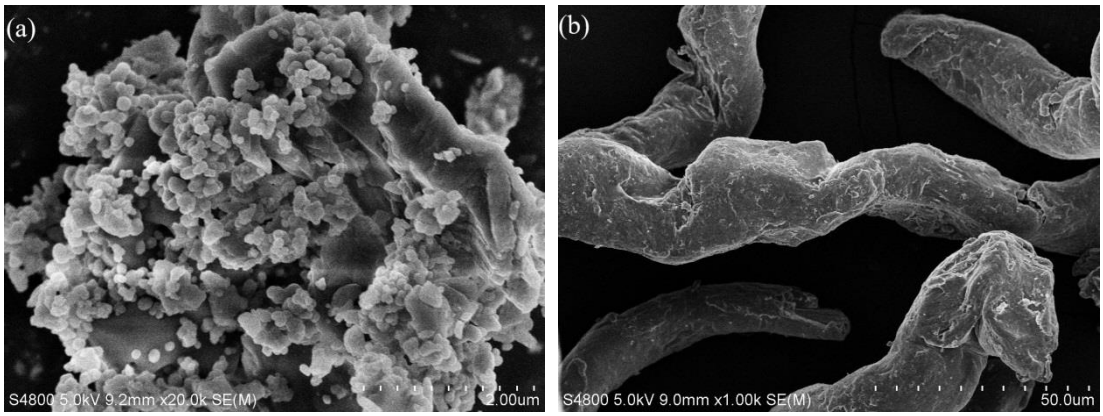

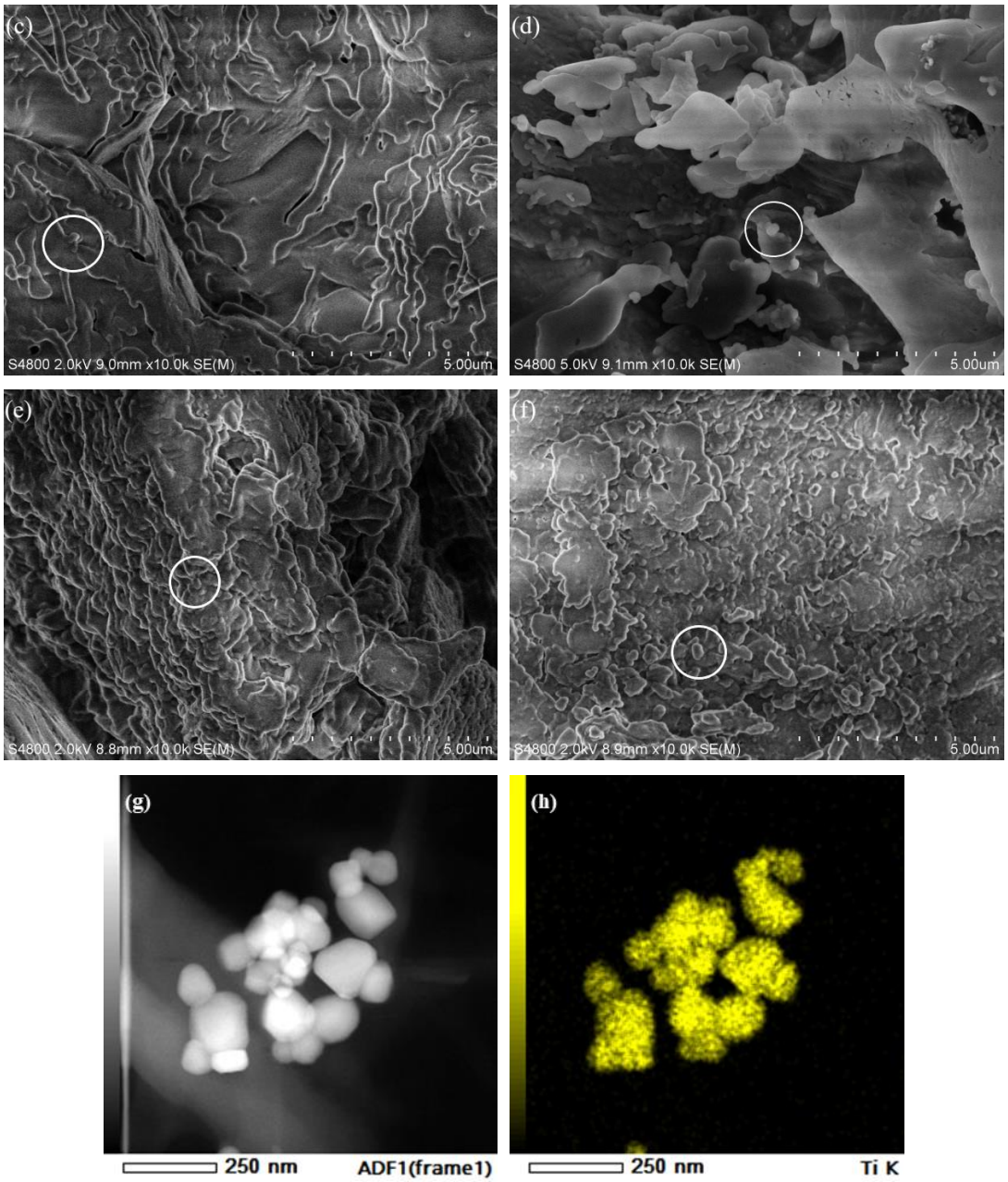


**Fig. 8.** SEM images of (a) $TiO_2$, (b) CMC, (c) LA-HD/$TiO_2$, (d) MA-HD/$TiO_2$, (e) PA-HD/$TiO_2$ (f) SA-HD/$TiO_2$ and EDS-mapping results of (g) MA-HD/$TiO_2$ and (h) Ti.

### 3.4. Phase change properties

Phase change properties of fatty acids (i.e., LA, MA, PA and SA), HD, EMs (i.e., LA-HD, MA-HD, PA-HD and SA-HD) and CPCMs (i.e., LA-HD/$TiO_2$, MA-HD/$TiO_2$, PA-HD/$TiO_2$ and SA-HD/$TiO_2$) are characterized by DSC. As the theoretical calculations for EMs in this paper are closely related to the data on the melting process, it is necessary to analyze the melting process for all samples. The DSC curves of LA, MA, PA, SA, HD, EMs and corresponding CPCMs are illustrated in Fig. 9. The corresponding data of extrapolated peak onset temperature ($T_e$), melting peak temperature ($T_m$) and enthalpy of melting ($\Delta H_m$) and CV% are summarized in Table 6. $T_m$ is the phase transition temperature during melting process. The phase transition temperature and the enthalpy of melting for PCM both increase with the growth of molecular length/size. The phase transition temperature of EMs is significantly lower than those of its two components, due to the

weakly attractive interaction between the different components of EMs [23, 44]. This phase transition temperature is known as the eutectic point. Amongst the prepared EMs, for LA-HD, the phase transition temperature is 47.6 ℃, which is lower than those of LA and HD for about 7.21% and 18.91% respectively. The phase transition temperature of MA-HD is 50.9 ℃, which is 19.60% and 13.30% lower than those of MA and HD respectively. The phase transition temperature of PA-HD is lower than those of PA and HD for about 20.03% and 5.45%. The phase transition temperature of SA-HD is 26.68% lower than that of SA while it is 3.07% lower than that of HD. In addition, due to the mixing of the lower enthalpy components in the EMs, the overall enthalpy of the composite will be lower than that of the higher enthalpy component. This result is similar in the trends which published early for EM [24, 25]. After mixing, the melting enthalpy of the EMs decreases relative to the higher enthalpy components, but still maintains high values, which is greater than 200 J/g. It indicates that the EMs of fatty acids/1-hexadecanol can effectively broaden the range of phase transition temperature suitable for this class of organics and preserve the good thermal feature of individual component. Different EMs can be utilized as needed, allowing for a wider range of applications for fatty acids and fatty alcohols. Comparing the thermal properties of binary EMs obtained from DSC test with that computed by theoretical calculation in Section 2.2.1, the deviation is small and within an acceptable range. It also indicates that the Schrader equation can be used for calculation related to the EMs of fatty acids/1-hexadecanol.

Amongst the DSC curves of CPCMs, they all have only one endothermic peak with a peak shape similar to that of the corresponding EMs respectively. The phase transition temperatures of LA-HD/$TiO_2$, MA-HD/$TiO_2$, PA-HD/$TiO_2$ and SA-HD/$TiO_2$ are 45.4 ℃, 51.2 ℃, 55.1 ℃ and 58.3 ℃, which vary only 4.62%, 0.59%, 0.72% and 2.46% with those of EMs respectively. For the prepared CPCM, the enthalpy of melting alters slightly with respect to that of EM. The small changes in phase transition temperature and enthalpy of melting demonstrated that the strong physical interaction between EMs and $TiO_2$ in CPCMs. The tiny decrease of latent heat does not affect the energy storage capacity of PCMs obviously. On the contrary, as more thermal energy can be obtained in a short time due to $TiO_2$, the heat absorption and release capacities of CPCMs will be higher than those of EMs.

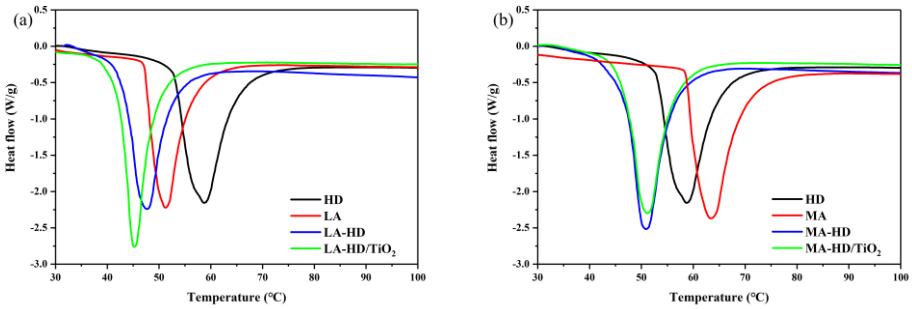

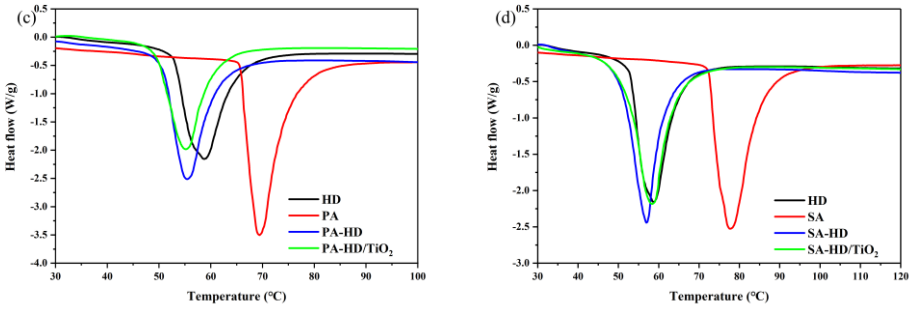


**Fig. 9.** The DSC curves of (a) HD, LA, LA-HD and corresponding CPCM, (b) HD, MA, MA-HD and corresponding CPCM, (c) HD, PA, PA-HD and corresponding CPCM and (d) HD, SA, SA-HD and corresponding CPCM.

**Table 6**

Thermal performance of LA, MA, PA, SA, HD, EMs and corresponding CPCMs.

| Sample | $T_e$ (℃) | $T_m$ (℃) | $\Delta H_m$ (kJ/g) | *CV* (%) |
|---|---|---|---|---|
| LA | 47.2±0.1 | 51.3±0.1 | 0.19 | 3.72 |
| MA | 58.6±0.1 | 63.3±0.1 | 0.20 | 2.21 |
| PA | 65.7±0.1 | 69.4±0.1 | 0.24 | 3.52 |
| SA | 72.4±0.1 | 77.6±0.1 | 0.24 | 2.24 |
| HD | 52.9±0.1 | 58.7±0.1 | 0.22 | 3.77 |
| LA-HD | 41.8±0.1 | 47.6±0.1 | 0.20 | 2.26 |
| MA-HD | 46.8±0.1 | 50.9±0.1 | 0.21 | 2.66 |
| PA-HD | 50.7±0.1 | 55.5±0.1 | 0.22 | 2.05 |
| SA-HD | 51.1±0.1 | 56.9±0.1 | 0.22 | 3.21 |
| LA-HD/$TiO_2$ | 42.2±0.1 | 45.4±0.1 | 0.20 | 2.21 |
| MA-HD/$TiO_2$ | 47.0±0.1 | 51.2±0.1 | 0.20 | 2.68 |
| PA-HD/$TiO_2$ | 49.5±0.1 | 55.1±0.1 | 0.21 | 2.15 |
| SA-HD/$TiO_2$ | 52.3±0.1 | 58.3±0.1 | 0.22 | 2.54 |

3.5. Thermal reliabilities of phase change materials

The prepared CPCMs should retain stable thermal properties after a certain number of thermal cycles. The thermal reliability can be tested by thermal cycling test. Fig. 10 shows the DSC curves of CPCMs before and after thermal cycling. The thermal properties and CV% are documented in Table 7. The shapes of endothermic peaks before and after thermal cycling are similar. The phase transition temperatures of CPCMs after 100 thermal cycles are 45.4 ℃, 47.6 ℃, 53.4 ℃ and 54.8 ℃ for LA-HD/$TiO_2$, MA-HD/$TiO_2$, PA-HD/$TiO_2$ and SA-HD/$TiO_2$ respectively, which are 0, 7.03%, 3.09% and 6.00% changed relative to the phase transition temperatures before thermal cycling. In addition, the enthalpy of melting varies slightly before and after thermal cycling, especially the LA-HD/$TiO_2$. The prepared MA-HD/$TiO_2$ is still used as an example to further verify the thermal reliabilities of the CPCMs. FTIR analysis is carried out on the sample after 100 thermal cycles. Fig. 11 exhibits the FTIR spectra of MA-HD/$TiO_2$ before and after thermal cycling. It showed that the characteristic peaks fall on the same functional group, which implies that no chemical interaction occurs even after 100 thermal cycles. Two different parts (part A and part B) of sample are selected for EDS-mapping after 100 thermal cycles as shown in Fig. 12. It can be clearly observed that $TiO_2$ is still well distributed in the field of view of sample taken. Therefore,

403 the thermal cycling test proves that the CPCMs have good thermal reliabilities.

404

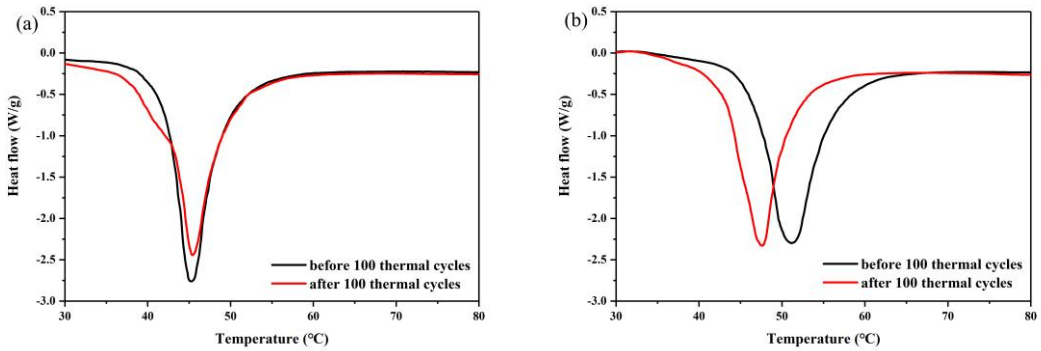


405

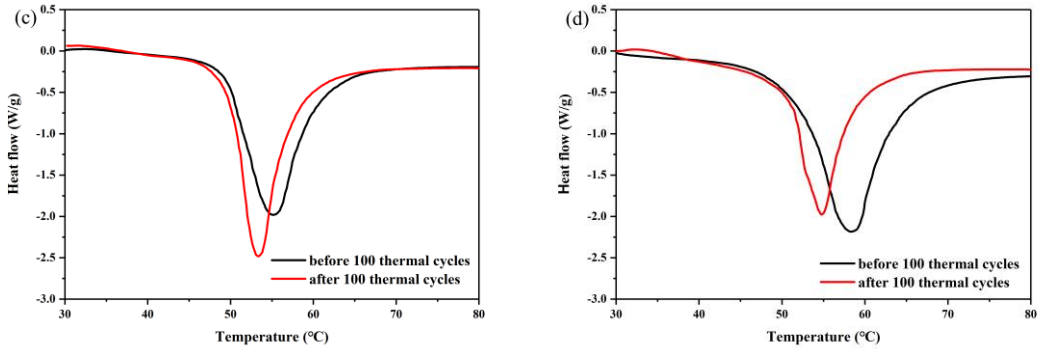


406 **Fig. 10.** DSC curves of (a) LA-HD/$TiO_2$, (b) MA-HD/$TiO_2$, (c) PA-HD/$TiO_2$ and (d) SA-HD/$TiO_2$
407 before and after 100 thermal cycles.

408 **Table 7**

409 Thermal performance of CPCMs before and after 100 thermal cycles.

| Sample | Cycling number | $T_m$ (℃) | $\Delta H_m$ (kJ/g) | $CV$ (%) |
|---|---|---|---|---|
| LA-HD/$TiO_2$ | 0 | 45.4±0.1 | 0.20 | 2.21 |
| | 100 | 45.4±0.1 | 0.20 | 4.23 |
| MA-HD/$TiO_2$ | 0 | 51.2±0.1 | 0.20 | 2.68 |
| | 100 | 47.6±0.1 | 0.20 | 3.54 |
| PA-HD/$TiO_2$ | 0 | 55.1±0.1 | 0.21 | 2.15 |
| | 100 | 53.4±0.1 | 0.21 | 3.37 |
| SA-HD/$TiO_2$ | 0 | 58.3±0.1 | 0.22 | 2.54 |
| | 100 | 54.8±0.1 | 0.22 | 2.05 |

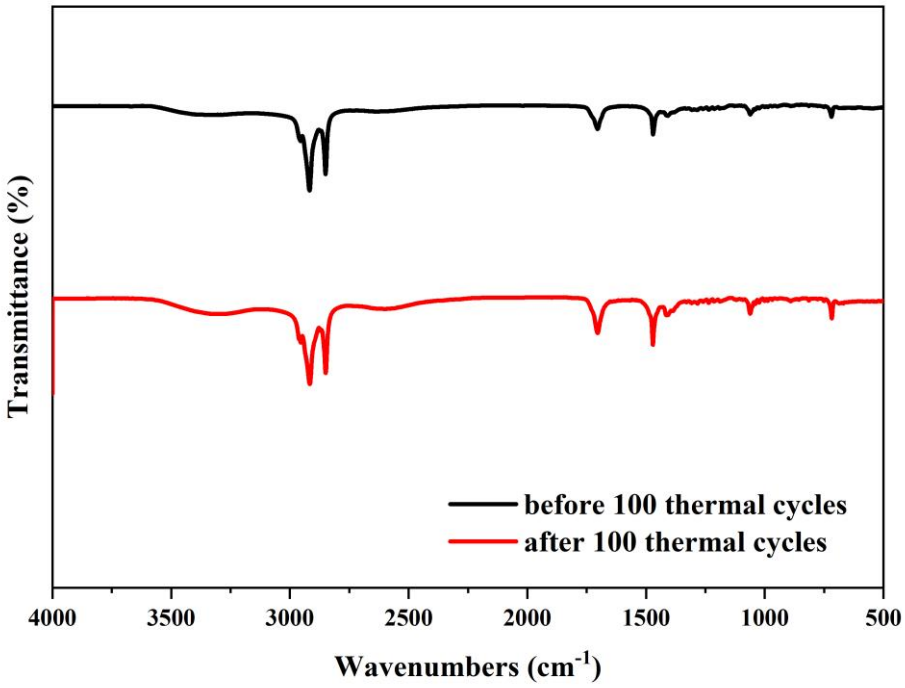


410

411 **Fig. 11.** The FTIR results of MA-HD/$TiO_2$ before and after 100 thermal cycles.

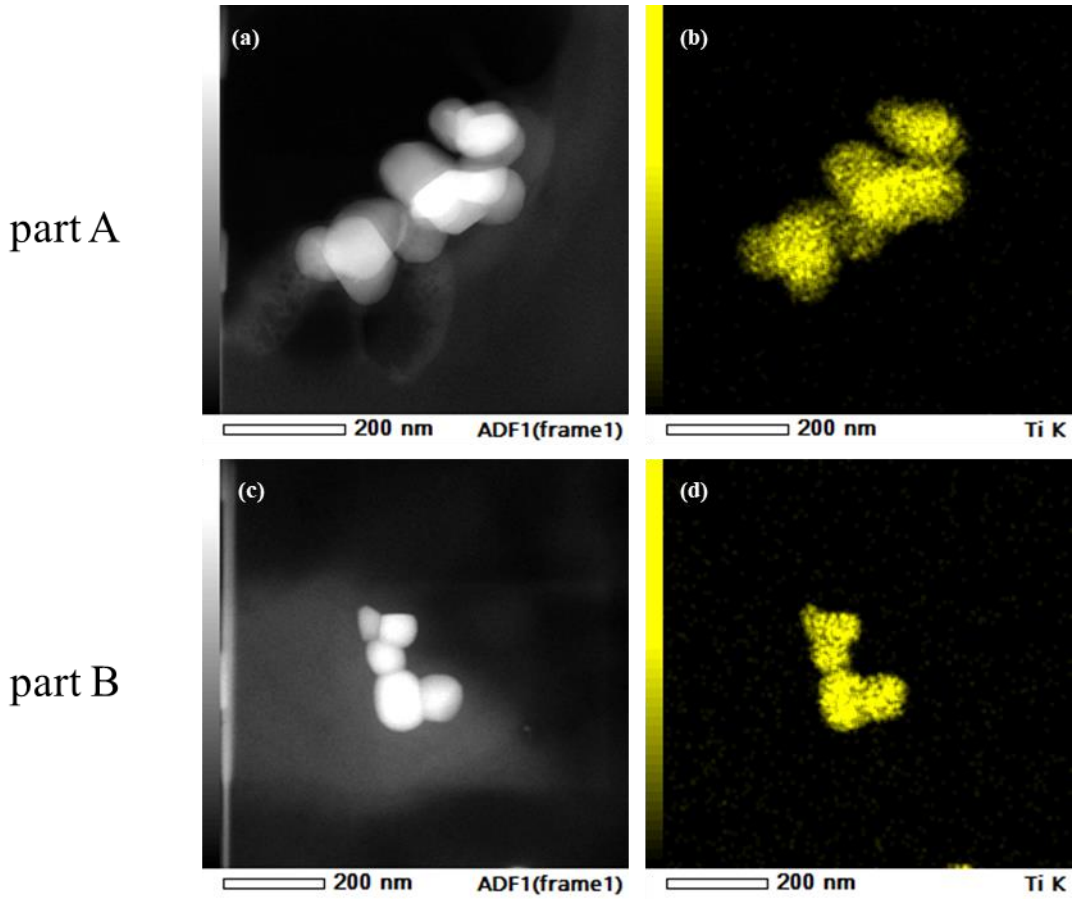


412

413 **Fig. 12.** The EDS-mapping results with (a-b) part A and (c-d) part B of MA-HD/$TiO_2$ after 100
414 thermal cycles.

### 3.6. Thermal stabilities of phase change materials

The TGA is adopted to evaluate the thermal stabilities of PCMs. The TGA curves of LA, MA, PA, SA, HD, EMs and corresponding CPCMs are displayed in Fig. 13. The corresponding data of the temperature of starting mass loss ($T_{on}$) and the temperature of decomposing completely ($T_{off}$) are listed in Table 8. Combining experimental results with theory and errors for analyze. For the LA, MA, PA, SA and HD, the mass losses occur at the temperature between 154.7 ℃ and 306.8 ℃. The mass losses for EMs (i.e., LA-HD, MA-HD, PA-HD and SA-HD) occur at the temperature between 159.6 ℃ and 290.8 ℃. The weight losses are chiefly caused by the gasification of single fatty acid and HD and the thermal degradation of EMs.

There is only a small mass loss (0.1 wt.%) below 189.2 ℃ for the SA-HD/$TiO_2$, and other CPCMs also possess strong resistance to decomposition. In the temperature range of 50-400 ℃, the maximum mass losses are 100 wt.% for EMs but less than 100% for CPCMs. This is attributed by the residual carbonized CMC and indecomposable $TiO_2$ in the CPCMs. The complete decomposing temperatures of MA-HD/$TiO_2$, PA-HD/$TiO_2$ and SA-HD/$TiO_2$ are 307.7 ℃, 341.1 ℃ and 333.8 ℃ respectively, which are delayed by 13.75%, 27.94% and 14.79% relative to those of corresponding EMs. Thus the temperature tolerable range is significantly expanded. In addition, the decomposition processes of CPCMs are significantly prolonged compared with those of EMs. For example, the temperature range of PA-HD degradation process is 166.2-266.6 ℃ while that of PA-HD/$TiO_2$ is 168.8-341.1 ℃, which is prolonged by 71.61%. The reason for this result is that the addition of particles in the base material has served as the thermal retardant against the temperature, which would delay the decomposition of base material [45]. Therefore, the TGA test proves that the CPCMs have good thermal stabilities.

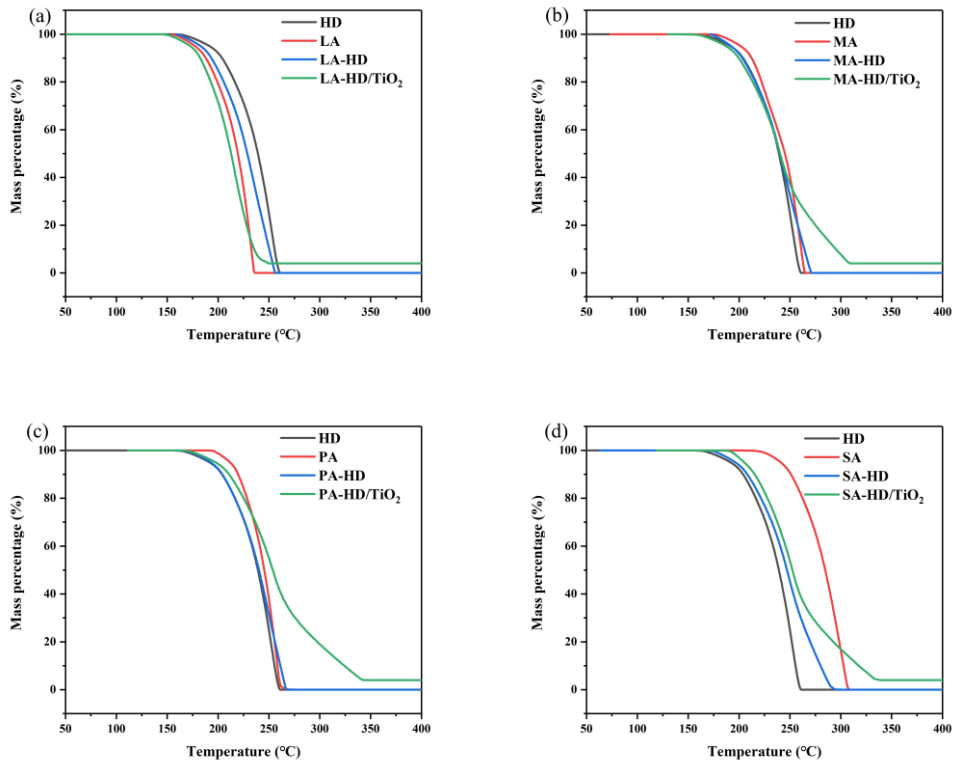


**Fig. 13.** The TGA curves of (a) HD, LA, LA-HD and corresponding CPCM, (b) HD, MA, MA-HD and corresponding CPCM, (c) HD, PA, PA-HD and corresponding CPCM and (d) HD,

SA, SA-HD and corresponding CPCM.

**Table 8**

Thermal stabilities of LA, MA, PA, SA, HD, EMs and corresponding CPCMs.

| Sample | $T_{on}$ (℃) | $T_{off}$ (℃) |
|---|---|---|
| LA | 154.7±0.1 | 235.2±0.1 |
| MA | 175.5±0.1 | 264.2±0.1 |
| PA | 193.8±0.1 | 261.1±0.1 |
| SA | 214.3±0.1 | 306.8±0.1 |
| HD | 161.7±0.1 | 258.8±0.1 |
| LA-HD | 159.6±0.1 | 255.8±0.1 |
| MA-HD | 172.6±0.1 | 270.5±0.1 |
| PA-HD | 166.2±0.1 | 266.6±0.1 |
| SA-HD | 172.6±0.1 | 290.8±0.1 |
| LA-HD/$TiO_2$ | 147.5±0.1 | 236.2±0.1 |
| MA-HD/$TiO_2$ | 157.5±0.1 | 307.7±0.1 |
| PA-HD/$TiO_2$ | 168.8±0.1 | 341.1±0.1 |
| SA-HD/$TiO_2$ | 189.2±0.1 | 333.8±0.1 |

### 3.7. Thermal conductivities of phase change materials

The thermal conductivities of EMs and their corresponding CPCMs are exhibited in Fig. 14. The thermal conductivity of PA-HD/$TiO_2$ reaches 0.358 W/(m·K), which is the highest among the prepared EMs and CPCMs. $TiO_2$ plays a major role in improving the thermal conductivity, but it is governed by the phonon propagation. The augment in thermal conductivity of CPCMs is limited because of increased defects caused by CMC. The CMC can lead to the scattering of phonons, which causes the decrease of thermal conductivity [46]. Nevertheless, the thermal conductivities of CPCMs are still higher than those of EMs. The thermal conductivities of LA-HD/$TiO_2$, MA-HD/$TiO_2$, PA-HD/$TiO_2$ and SA-HD/$TiO_2$ are 24.73%, 8.47%, 11.70% and 14.28% higher than those of their EMs respectively, which makes PCMs more suitable for thermal energy storage.

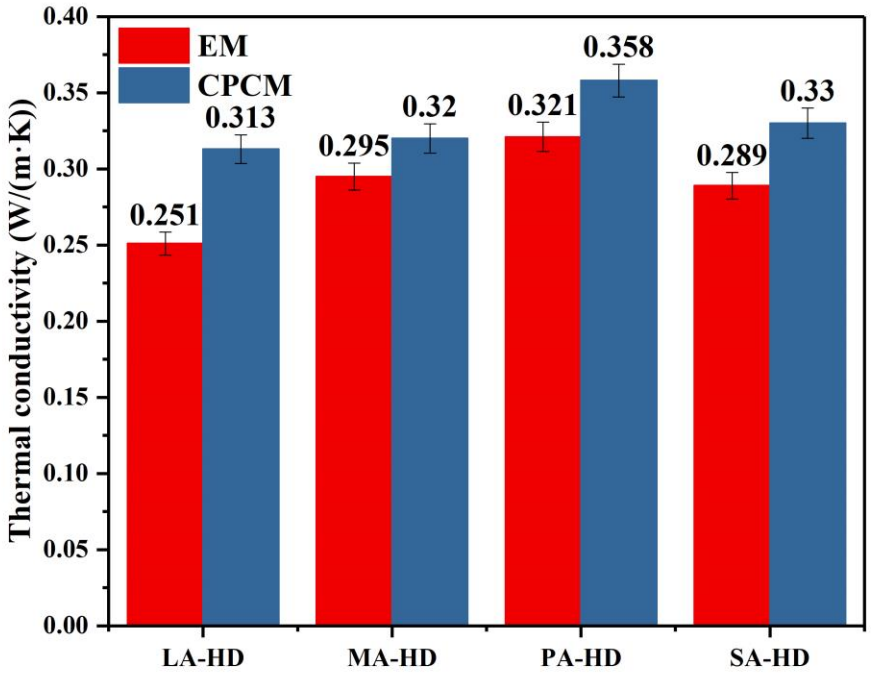


**Fig. 14.** Thermal conductivities of EMs and their CPCMs.

## 4. Conclusions

In this paper, fatty acids/1-hexadecanol binary eutectic CPCMs are developed. The mass ratios of the components and the thermal properties of binary EMs are firstly determined by theoretical calculation. The accuracy of the theoretical calculation is then verified experimentally. The optimal content of the additive is determined experimentally. 2 wt.% $TiO_2$ is added to improve the thermal conductivities of EMs. The chemical structure, microscopic morphology, thermal storage property, thermal reliability and thermal stability of the materials are tested using FTIR, SEM, DSC, thermal cycling test and TGA respectively. The thermal conductivities of the EMs and corresponding CPCMs are also measured. The FTIR and SEM results show that there is no chemical reaction occurred within the CPCMs and $TiO_2$ is dispersed in the EMs without aggregation. The results of DSC test illustrate that the phase transition temperatures are 45.4 ℃, 51.2 ℃, 55.1 ℃ and 58.3 ℃ for LA-HD/$TiO_2$, MA-HD/$TiO_2$, PA-HD/$TiO_2$ and SA-HD/$TiO_2$ respectively. The EM-based CPCMs with high latent heat above 200 J/g effectively broaden the phase transition temperature range of individual fatty acids and fatty alcohols. The thermal conductivities of EMs are all heightened after the addition of $TiO_2$. Thermal cycling test results indicate that the thermal energy storage/release properties of CPCMs possess better repeatability. The TGA test reveals that the CPCMs exhibit good thermal stability in the operating temperature range for most thermal applications.

The novel CPCMs proposed in present work, which are with simple preparation method, suitable phase transition temperature, high latent heat, good thermal reliability, dependable thermal stability and high thermal conductivity, are up-and-coming potentials for thermal energy storage. The methodology followed to explore the fatty acids and fatty alcohols EM-based CPCMs

in the present research can provide reference for researchers and engineers in the selection and utilization of the PCMs for energy storage.

## Declaration of competing interest

None.


## Acknowledgements

This work was supported by the Shandong Energy Institute (No. SEI-I202125), the Shandong Provincial Natural Science Foundation (No. ZR2018PEE017), the Application Foundation Research Program of Qingdao (No. 17-1-1-17-jch) and the National Natural Science Foundation of China (No. 21808235).


## References


[1] S. Doakhan, M. Montazer, A. Rashidi, R. Moniri, M.B. Moghadam, Influence of sericin/$TiO_2$ nanocomposite on cotton fabric: Part 1. Enhanced antibacterial effect, Carbohyd. Polym. 94 (2) (2013) 737-748.

[2] R. Aladpoosh, M. Montazer, The role of cellulosic chains of cotton in biosynthesis of ZnO nanorods producing multifunctional properties: Mechanism, characterizations and features, 126 (2015) 122-129.

[3] M. Taheri, M. Montazer, A.B. Rezaie, A. Minuchehr, M. Aghaie, A Cleaner Affordable Method for Production of Bactericidal Textile Substrates by in situ Deposition of ZnO/Ag Nanoparticles, Fiber. Polym. 22 (2021) 2792-2802.

[4] S. Li, Z. Liu, X. Wang, A comprehensive review on positive cold energy storage technologies and applications in air conditioning with phase change materials, Appl. Energy 255 (2019) 113667.

[5] S. Zhang, D.L. Feng, L. Shi, L. Wang, Y.A. Jin, L.M. Tian, Z.Y. Li, G.Y. Wang, L. Zhao, Y.Y. Yan, A review of phase change heat transfer in shape-stabilized phase change materials (ss-PCMs) based on porous supports for thermal energy storage, Renew. Sust. Energ. Rev. 135 (2021) 110127.

[6] S.M.H. Zadeh, S.A.M. Mehryan, M. Ghalambaz, M. Ghalambaz, M. Ghodrat, J. Young, A. Chamkha, Hybrid thermal performance enhancement of a circular latent heat storage system by utilizing partially filled copper foam and Cu/GO nano-additives, Energy 213 (2020) 118761.

[7] G.J. Zhang, L. Wang, S. Zhang, Y.M. Li, Z.N. Zhou, Effect evaluation of a novel dehumidification structure based on the modified model, Energ. Convers. Manage. 159 (2018) 65-75.

[8] W.Z. Jin, L.H. Jiang, L. Chen, Y. Gu, M.Z. Guo, L. Han, X.Q. Ben, H.H. Yuan, Z.X. Lin, Preparation and characterization of capric-stearic acid/montmorillonite/graphene composite phase change material for thermal energy storage in buildings, Constr. Build. Mater. 301 (2021) 124102.

[9] X. Qiao, X.F. Kong, L. Wang, Thermal performance analysis of a thermal enhanced form-stable composite phase change material with aluminum nitride, Appl. Therm. eng. 187 (2021) 116581.

[10] N. Akram, M.U. Moazzam, H.M. Ali, A. Ajaz, A. Saleem, M. Kilic, A. Mobeen, Improved waste heat recovery through surface of kiln using phase change material. Thermal Science, 22(2) (2018) 1089-1098.

[11] X.S. Du, J.H. Qiu, S. Deng, Z.L. Du, X. Cheng, H.B. Wang, Flame-retardant and solid-solid phase change composites based on dopamine-decorated BP nanosheets/Polyurethane for efficient solar-to-thermal energy storage, Renew. Energ. 164 (2021) 1-10.

[12] M. Al-Jethelah, S.H. Tasnim, S. Mahmud, A. Dutta, Nano-PCM filled energy storage system for solar-thermal applications, Renew. Energ. 126 (2018) 137-155.

[13] A. Kumar, S.K. Saha, Performance study of a novel funnel shaped shell and tube latent heat thermal energy storage system, Renew. Energ. 165(P1) (2021) 731-747.

[14] M. Montazer, A. Keshvari, P. Kahali, Tragacanth gum/nano silver hydrogel on cotton fabric: In-situ synthesis

and antibacterial properties, Carbohyd. Polym. 154 (2016) 257-266.
[15] A. E. Chimeh, M. Montazer, A. Rashidi, Conductive and photoactive properties of polyethylene terephthalate fabrics treated with nano $TiO_2$/nano carbon blacks, New Carbon Mater. 28 (4) (2013) 313-320.
[16] A.B. Rezaie, M. Montazer, M.M. Rad, Facile fabrication of cytocompatible polyester fiber composite incorporated via photocatalytic nano copper ferrite/myristic-lauric fatty acids coating with antibacterial and hydrophobic performances, Mat. Sci. Eng. C-Mater. 104 (2019) 109888.
[17] M.M. Kenisarin, Thermophysical properties of some organic phase change materials for latent heat storage. A review, Sol. Energy 107 (2014) 553-575.
[18] Y.P. Yuan, N. Zhang, W.Q. Tao, X.L. Cao, Fatty acids as phase change materials: A review. Renew. Sust. Energ. Rev. 29 (2014) 482-498.
[19] A.B. Rezaie, M. Montazer, Shape-stable thermo-responsive nano $Fe_3O_4$/fatty acids/PET composite phase-change material for thermal energy management and saving applications, Appl. Energ. 262 (2020) 114501.
[20] B.E. Jebasingh, A.V. Arasu, Characterisation and stability analysis of eutectic fatty acid as a low cost cold energy storage phase change material, J. Energy Storage 31 (2020) 101708.
[21] A.B. Rezaie, M. Montazer, The prepared composites can be utilized for low temperature energy storage/release systems, Appl. Energ. 228 (2019) 1911-1920.
[22] G. Hekimoğlu, M. Nas, M. Ouikhalfan, A. Sarı, Ş. Kurbetci, V.V. Tyagi, R.K. Sharma, T.A. Saleh, Thermal management performance and mechanical properties of a novel cementitious composite containing fly ash/lauric acid-myristic acid as form-stable phase change material, Constr. Build. Mater. 274 (2021) 122105.
[23] Y.B. Cai, G.Y. Sun, M.M. Liu, J. Zhang, Q.Q. Wang, Q.F. Wei, Fabrication and characterization of capric-lauric-palmitic acid/electrospun $SiO_2$ nanofibers composite as form-stable phase change material for thermal energy storage/retrieval, Sol. Energy 118 (2015) 87-95.
[24] H.T. Wei, X.Z. Xie, X.Q. Li, X.S. Lin, Preparation and characterization of capric-myristic-stearic acid eutectic mixture/modified expanded vermiculite composite as a form-stable phase change material, Appl. Energ. 178 (2016) 616-623.
[25] N. Philip, G.R. Dheep, A. Sreekumar, Cold thermal energy storage with lauryl alcohol and cetyl alcohol eutectic mixture: Thermophysical studies and experimental investigation, J. Energy Storage 27 (2020) 101060.
[26] N. Philip, C. Veerakumar, A. Sreekumar, Lauryl alcohol and stearyl alcohol eutectic for cold thermal energy storage in buildings: preparation, thermophysical studies and performance analysis, J. Energy Storage 31 (2020) 101600.
[27] X. Liu, Experimental study on the preparation and properties of composite phase change materials, University of Science and Technology of Suzhou 2019.
[28] T.P. Teng, C.C. Yu, Characteristics of phase-change materials containing oxide nano-additives for thermal storage, Nanoscale Res. Lett. 7(1) (2012) 1-10.
[29] S. Harikrishnan, M. Deenadhayalan, S. Kalaiselvam, Experimental investigation of solidification and melting characteristics of composite PCMs for building heating application, Energ. Convers. Manage. 86 (2014) 864-872.
[30] S. Kalaiselvam, R. Parameshwaran, S. Harikrishnan, Analytical and experimental investigations of nanoparticles embedded phase change materials for cooling application in modern buildings, Renew. Energ. 39(1) (2011) 375-387.
[31] R.K. Sharma, P. Ganesan, V.V. Tyagi, H.S.C. Metselaar, S.C. Sandaran, Thermal properties and heat storage analysis of palmitic acid-$TiO_2$ composite as nano-enhanced organic phase change material (NEOPCM), Appl. Therm. Eng. 99 (2016) 1254-1262.
[32] J.X. Wang, Preparation and thermal conductivity study of binary organic composite phase change thermal storage materials, Jiangnan University 2019.

[33] I. Chriaa, M. Karkri, A. Trigui, I. Jedidi, M. Abdelmouleh, C. Boudaya, The performances of expanded graphite on the phase change materials composites for thermal energy storage, Polymer 212 (2021) 123128.
[34] D.G. Atinafu, S. Wi, B.Y. Yun, S. Kim, Engineering biochar with multi walled carbon nanotube for efficient phase change material encapsulation and thermal energy storage, Energy 216 (2021) 119294.
[35] M. Liu, C. Zhang, Z.J. Du, W. Zou, Fabrication of shape-stabilized phase change materials with melamine foam/multi-walled carbon nanotubes composite as container, Compos. Interface. 28(3) (2021) 255-271.
[36] G.R. Dheep, A. Sreekumar, Influence of nanomaterials on properties of latent heat solar thermal energy storage materials-A review, Energ. Convers. Manage. 83 (2014) 133-148.
[37] S. Wi, S. Yang, J.H. Park, S. J. Chang, S. Kim, Climatic cycling assessment of red clay/perlite and vermiculite composite PCM for improving thermal inertia in buildings, Build. Environ. 167 (2020) 106464.
[38] Z.W. Yang, J.H. Li, X.Z. Luan, S. Song, Effects of acid leaching and organic intercalation on the thermophysical properties of paraffin/expanded vermiculite composite phase change materials, Appl. CLAY Sci. 196 (2020) 105754.
[39] M. Montazer, S. Morshedi, Nano photo scouring and nano photo bleaching of raw cellulosic fabric using nano $TiO_2$, Int. J. Biol. Macromol. 50 (4) 2012 1018-1025.
[40] L. Yang, N. Zhang, Y.P. Yuan, X.L. Cao, B. Xiang, Thermal performance of stearic acid/carbon nanotube composite phase change materials for energy storage prepared by ball milling, Int. J. Energ. Res. 43(12) (2019) 6327-6336.
[41] L. Wu, J.Q. Li, H. Wang, Y. Zhang, S.W. Feng, Y.C. Guo, J.L. Zhao, X.X. Wang, L.J. Guo, Experimental Investigation on Mechanism of Latent Heat Reduction of Sodium Acetate Trihydrate Phase Change Materials, Materials 13(3) (2020) 584-594.
[42] T.P. Teng, S.P. Yu, T.C. Hsiao, C.C Chung, I.A. Sahito, Study on the Phase Change Characteristics of Carbon-Based Nanofluids, J. Nanomater. 2018 (2018) 8230120.
[43] H.H. Mert, M.S. Mert, Preparation and characterization of encapsulated phase change materials in presence of gamma alumina for thermal energy storage applications, Thermochim. Acta 681 (2019) 178382.
[44] H.Z. Ke, Z.Y. Pang, B. Peng, J. Wang, Y.B. Cai, F.L. Huang, Q.F. Wei, Thermal energy storage and retrieval properties of form-stable phase change nanofibrous mats based on ternary fatty acid eutectics/polyacrylonitrile composite by magnetron sputtering of silver, J. Thermal. Anal. Calorim. 123(2) (2016) 1293-1307.
[45] M. Mehrali, S.T. Latibari, M. Mehrali, H.S.C. Metselaar, M. Silakhori, Shapestabilized phase change materials with high thermal conductivity based on paraffin/graphene oxide composite, Energ. Convers. Manage. 67 (2013) 275-282.
[46] C.C. Li, L.J. Fu, J. Ouyang, H.M. Yang, Enhanced performance and interfacial investigation of mineral-based composite phase change materials for thermal energy storage, Sci. Rep.-UK 3(1) (2013) 1908-1915.